Niobium uptake by [P8W48O184]40– macrocyclic polyanion

Journal:	*New Journal of Chemistry*
Manuscript ID	NJ-ART-04-2019-001907.R1
Article Type:	Paper
Date Submitted by the Author:	21-May-2019
Complete List of Authors:	Shmakova, Alexandra; Nikolaev Institute of Inorganic Chemistry Volchek, Victoria; Nikolaev Institute of Inorganic Chemistry SB RAS, ; Novosibirsk State University, Yanshole, Vadim ; International Tomography Center Siberian Branch of Russian Academy of Sciences , Group of Proteomics and Metabolomics; Novosibirsk State University, Department of Physics Kompankov, Nikolay; Nikolaev Institute of Inorganic Chemistry, Laboratory of Physical Chemistry of Condensed Matter martin, Nicolas; Oregon State University, Chemistry Nyman, May; Oregon State University, Chemistry Abramov, Pavel; Nikolaev Institute of Inorganic Chemistry, ; Novosibirsk State University, Sokolov, Maksim; Nikolaev Institute of Inorganic Chemistry, ; Novosibirsk State University, Natural Sciences

ARTICLE

Niobium uptake by $[P_8W_{48}O_{184}]^{40-}$ macrocyclic polyanion

Alexandra A. Shmakova, [a] Victoria V. Volchek, [a] Vadim Yanshole, [b,c] Nikolay B. Kompankov, [a] Nicolas P. Martin, [d] May Nyman, [d] Pavel A. Abramov,*[a,b] Maxim N. Sokolov [a,b]

Received 00th January 20xx,
Accepted 00th January 20xx

DOI: 10.1039/x0xx00000x

Reactions of inorganic macrocyclic polytungstate cavitands $K_{28}Li_5H_7[P_8W_{48}O_{184}]\cdot 92H_2O$ or $Li_{17}(NH_4)_{21}H_2[P_8W_{48}O_{184}]\cdot 85H_2O$ with $(NH_4)[NbO(C_2O_4)_2(H_2O)_2]\cdot 3H_2O$ (Nb-Ox) in aqueous solution lead to incorporation of up to five $\{NbO(H_2O)\}^{3+}$ units into the $\{P_8W_{48}\}$ cavity. The most stable species contain four $\{NbO(H_2O)\}^{3+}$ units. The uptake of $\{NbO(H_2O)\}^{3+}$ was determined by corroborative methods including single crystal XRD, inductively coupled plasma atomic emission spectroscopy (ICP-AES), ^{31}P and ^{13}C nuclear magnetic resonance (NMR), C-H-N elemental analysis (EA) and thermal gravimetric analysis (TGA). Solution speciation of the Nb-encapsulated macrocycles was studied by HPLC-ICP-AES and small angle X-ray scattering (SAXS).

Introduction

The main text of the article should appear here with headings as appropriate. The inorganic macrocyclic cavitand $[P_8W_{48}O_{184}]^{40-}$ $\{P_4W_{48}\}$ anion, which is composed of four $\{P_2W_{12}\}$ tetravacant Dawson-Wells lacunary units linked by capping tungsten atoms leading to a cyclic arrangement with a large (ca. 10 nm) internal cavity (Fig. 1) demonstrates an opportunity to coordinate different metal ions into its internal cavity as a controlled synthesis of heterometallic clusters. $\{P_4W_{48}\}$ is stable in water over large pH range (1-8), which greatly facilitates synthetic manipulation and compatibility with a wide variety of metal cations. This coordinative encapsulation has been demonstrated for various transition and post-transition metal cations including Sn^{2+},[1] Co^{2+},[2] or organometallic complexes.[3] Moreover $\{P_4W_{48}\}$ can stabilize polynuclear species, e.g. based on Cu^{2+} [4,5] or Ln^{3+}.[6] Reaction with Mn led to the formation of $\{Mn^{III}_{40}W^{VI}_{224}\}$ nanoscopic polyanion [7] with remarkable magnetic behavior. It can coordinate binuclear $\{Mo_2O_2S_2\}^{2+}$ molybdenum oxo-thio units, forming new chalco-POMs,[8] which were exploited as liquid crystals.[9] In some cases (Mn^{2+}), however, the cation ligation is restricted exclusively to the outer surface of $\{P_4W_{48}\}$; in this way Mn^{2+} linkers yielded three-dimensional extended frameworks.[10]

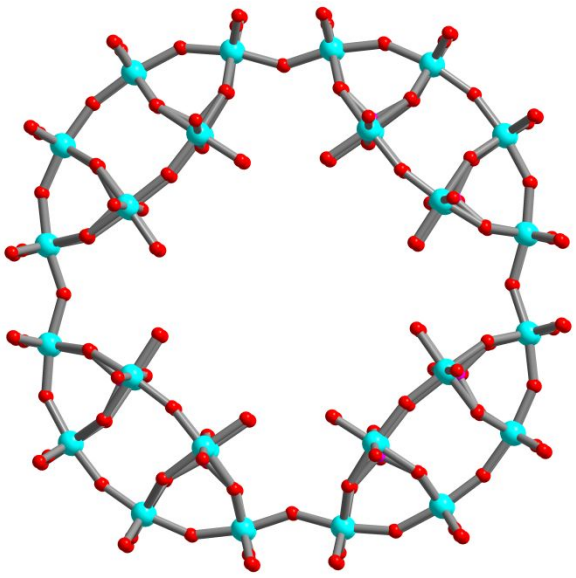

Figure 1. Structure of $[P_8W_{48}O_{184}]^{40-}$ macrocyclic anion. Tungsten atoms are cyan, oxo ligands are red.

The Nb-based polyoxometalates demonstrate unique properties owed to the distinctive characteristics of Nb(V). Due to its lower cationic charge, the Nb(V) site is expected to be less acidic, and the bonded oxide ligands more basic than corresponding Mo(VI) or W(VI)-oxo units. The diagonal relationship between Ti and Nb in the Periodic Table leads to similarities in the properties of their oxo-species, notably in the photocatalytic activity.[11–15] Moreover, inherently more

[a] *Nikolayev Institute of Inorganic Chemistry, 3 Akad. Lavrentiev Ave, 630090, Novosibirsk, Russia;*
[b] *Novosibirsk State University, Pirogova str. 2, 630090, Novosibirsk, Russia;*
[c] *International Tomography Center, Institutskaya str. 3a, 630090, Novosibirsk, Russia;*
[d] *Department of Chemistry Oregon State University,153 Gilbert Hall Corvallis, Oregon 97331-4003, USA.*
† Footnotes relating to the title and/or authors should appear here.
Electronic Supplementary Information (ESI) available: [Structural, HPLC-ICP-AES, NMR, SAXS, HR-ESI-MS data]. See DOI: 10.1039/x0xx00000x

basic homopolyoxoniobates and niobium-substituted POM tend to protonate in water, providing alkaline environment propitious for many catalytic and non-catalytic reactions, such as hydrolysis. This has been used to neutralize organophosphorus nerve agents by Nb-assisted basic hydrolysis.[16,17] Several types of mixed Nb-W POM have been prepared, including Nb-substituted Lindqvist $[Nb_xW_{6-x}O_{19}]^{(2+x)-}$ [18–20], Keggin $[XW_9Nb_3O_{40}]^{n-}$ (X = Si^{IV}, Ge^{IV}, n = 7; X = P^V, As^V, n = 6) [21–23] and Dawson $[P_2W_{12}(NbO_2)_6O_{56}]^{12-}$ [24], $[P_2W_{15}Nb_3O_{62}]^{9-}$ [25,26] and $[P_2W_{17}(NbO_2)O_{61}]^{7-}$ [27] polyoxotungstates. Some of these are photocatalytically active in oxidation [28] and reduction [29], and serve as pre-catalysts in hydrodesulfurization / isomerization processes [20], or as active catalysts for synthesis of polyalkylenepolyamines.[30] Some Nb-substituted Keggin heteropolytungstates show catalytic activity in olefin epoxidations [28,31–36]. The oxygen atom in the $\{NbO\}^{3+}$ unit, incorporated into a POM, is labile, and can be selectively replaced with O_2^{2-} or S^{2-} [37]. Nb(V) can be incorporated into polytungstate frameworks in various ways. In our ongoing research, focused on the study of group 5 polyoxometalates, we routinely use $(NH_4)[NbO(C_2O_4)_2(H_2O)_2]\cdot 3H_2O$ (Nb-Ox) as the niobium source for synthesis of Nb/W mixed POMs.[38–40] The advantages of using Nb-Ox as the Nb source include 1) easy control of the reaction stoichiometries since the oxalate complex is a stable solid of well-defined stoichiometry, and 2) the absence of hydrogen peroxide often used to solubilize Nb in more acidic conditions (peroxide-containing solutions are difficult to control).[31,41]

In this research we studied incorporation of $\{NbO\}^{3+}$ units into the macrocyclic $[P_8W_{48}O_{184}]^{40-}$ anion via reaction with the Nb-Ox reagent. Single-crystal X-ray diffraction, electrospray ionization mass spectrometry (ESI-MS), inductively coupled plasma atomic emission spectroscopy (ICP-AES), ^{31}P and ^{13}C nuclear magnetic resonance (NMR), C-H-N elemental analysis (EA) and thermal gravimetric analysis (TGA) and small-angle X-ray scattering (SAXS) were used to characterize the reaction products. Coordinated Nb(V) in $[P_8W_{48}O_{184}]^{40-}$ is within a confined cavity, yet it remains accessible. This may provide opportunity for selectivity in catalytic reactions. Moreover, the Nb-bound oxalate ligand (most of Nb is bound as $\{Nb(O)(C_2O_4)\}$) can be used for further functionalization or linking.

Results and Discussion

Synthesis

Two well-defined salts of the $\{P_4W_{48}\}$ macrocyclic anion, $K_{28}Li_5H_7[P_8W_{48}O_{184}]\cdot 92H_2O$ and $Li_{17}(NH_4)_{21}H_2[P_8W_{48}O_{184}]\cdot 85H_2O$ were used in the reactions with Nb-Ox in this study. All preparations were executed in aqueous solutions under gentle heating for two hours, followed by products crystallization at 5 °C. We used different Nb-Ox/$\{P_8W_{48}\}$ molar ratios (4:1, 8:1, 16:1) and different concentrations for better screening of the reaction products.

In the reaction of Nb-Ox with $K_{28}Li_5H_7[P_8W_{48}O_{184}]\cdot 92H_2O$, crystalline products were isolated and characterized by elemental analysis and TGA.

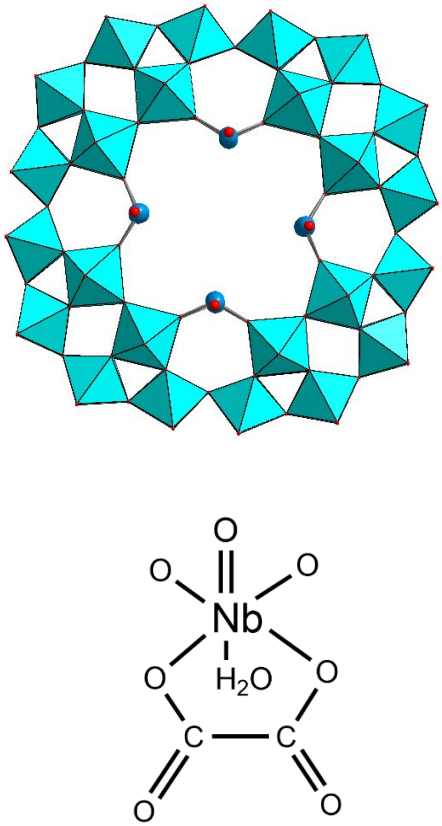

Figure 2. The first, common, type of Nb coordination to $\{P_8W_{48}\}$ and coordination environment of the encapsulated Nb (bottom). $\{WO_6\}$ octahedra are cyan, Nb atoms are blue, oxo ligands are red.

In all cases we found formation of a mixture of $K_xLi_yH_z[(P_8W_{48}O_{184})\{NbO(H_2O)\}_n]\cdot mH_2O$ (Table 1) compounds, differing in the number of coordinated $\{NbO(H_2O)\}^{3+}$ groups. Moreover, according to the elemental analysis and IR spectra, the isolated phases always contain oxalate anions, the number of which corresponds to the number of Nb ions, indicating the presence of the $\{NbO(C_2O_4)(H_2O)\}^+$ groups, with chelating oxalate occupying two free coordination sites of niobium (Fig. 2).

Increasing the Nb-Ox / $\{P_8W_{48}\}$ molar ratio four-fold raises the number of incorporated $\{NbO(C_2O_4)(H_2O)\}^+$ units from 1.7 (4:1) to 4.4 (16:1), while the number of suitable coordination sites of this type is eight (Fig. 2, left). This discrepancy means that coordination of niobium fragments might be hindered, perhaps by competition with K^+, residing in the cage, for the same coordination sites (Fig. 2, top). Increasing the concentration at the same molar ratio does not increase the uptake of $\{NbO(C_2O_4)(H_2O)\}^+$ (Tables 1, 2). In the case of the more soluble, potassium-free lithium-ammonium salt, $Li_{17}(NH_4)_{21}H_2[P_8W_{48}O_{184}]\cdot 85H_2O$, crystallization of the products takes more time. Nevertheless, elemental analysis and TGA

again give evidence for the formation of a mixture of $Li_x(NH_4)_yH_z[(P_8W_{48}O_{184})\{NbO(H_2O)\}_n]\cdot mH_2O$ compounds with different n values. Raising the {Nb-Ox}/{P_8W_{48}} ratio increases the number of the encapsulated $\{NbO(H_2O)\}^+$ groups from 2.8 (4:1) to 5 (16:1), indicating a somewhat more favorable incorporation of Nb(V) due to weaker interaction of Li^+/NH_4^+ cations in the cavity with the anion. Elemental analysis indicates presence of the oxalate ligands, but the number of $C_2O_4^{2-}$ is slightly less than total number of Nb atoms. This hints at possible presence of additional niobium in the structure, coordinated in a different mode, bearing no oxalate ligands.

Crystal structure

We determined the structure of the product isolated from the reaction with $Li_{17}(NH_4)_{21}H_2[P_8W_{48}O_{184}]\cdot 85H_2O$ with 30 eq. of {Nb-Ox} (**1**). The crystal structure of **1** is built of the macrocyclic anions {P_8W_{48}}, decorated by $\{NbO(H_2O)\}^{3+}$ groups in two different coordination environments. The predominant coordination sites are inside the central cavity ("common" site with octahedral coordination, Fig. 2) which contain 3.2 $\{NbO(H_2O)(C_2O_4)\}^{3+}$ units randomly distributed over eight equivalent positions, available for coordination). These "common" positions are routinely occupied by other d- and p-cations.[1–5] Each Nb atom bridges two adjacent {P_2W_{12}} moieties in such a way as to form rings of four {WO_6} octahedra and one octahedral {NbO_6} unit (Fig. 2, top).

Due to disorder in the location of the $\{NbO(H_2O)\}^{3+}$ units were not able to refine full coordination environment around Nb. However, from elemental analysis and NMR (see below) we assume that all oxalates are coordinated to Nb residing in these "common" positions, thus arriving at the total count of 3.2 $\{NbO(C_2O_4)(H_2O)\}^+$ units inside the central cavity. The situation is actually more complex from the structural point of view, since at each site there are two orientations of the O=Nb-OH_2 vector, which has a shorter Nb=O bond and a longer Nb-OH_2 bond, with the Nb=O bond pointing either into or out of the cavity. This brings about two non-equivalent positions (Nb1 and Nb2, correspondingly) in each of the eight equivalent sites, with relative occupancies 0.25(Nb1) and 0.15(Nb2). The bond distances Nb1-O1 (1.76(4) Å) and Nb1-O2 (2.56(4) Å) are close to the values expected for Nb=O and Nb-H_2O, respectively, even if for Nb2 the match is less satisfactory due to overlapping positions of oxygen atoms.

In the refinement, some extra electron density (3.5 e) appears also in the pentagonal positions between the {P_2W_{12}} units. There are eight such positions in each {P_8W_{48}} anion (Fig. 3). The pentagonal coordination environment clearly rules out a water molecule or ammonium cation as the source of this extra density. Refinement as partially occupied by Nb gives occupancy around 5% (0.4 $\{NbO(H_2O)\}^{3+}$ per anion) with Nb3-O4 = 2.22(4) Å and Nb3-O15 = 2.23(4) Å. These distances are the average of the expected Nb=O and Nb-H_2O distances, due to overlap of the multiple positions of O-atoms because of two alternative orientations of the O=Nb-OH_2 vector. The central Nb atoms plus four {WO_6} polyhedra create an open pentagonal building block (Fig. 3, bottom) akin to the pentagonal {$Mo(Mo_5)$} units, essential for assembly of giant ring- and capsule polymolybdates.[42,43]

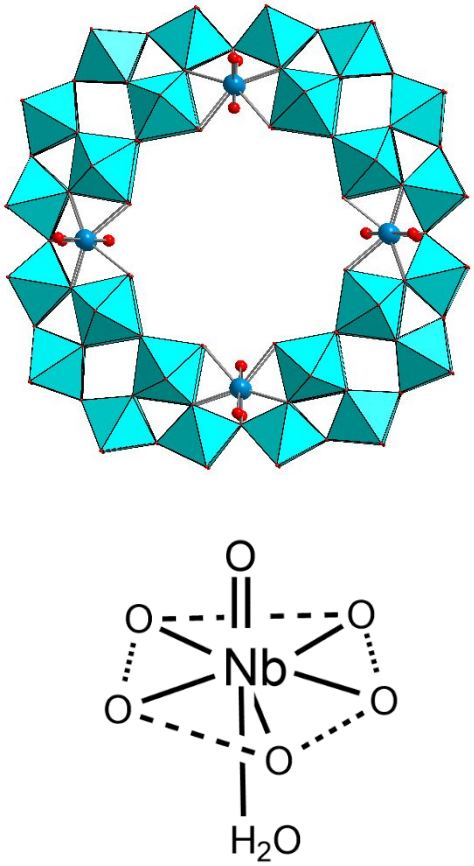

Figure 3. The second type of Nb coordination (up), and the coordination environment of the encapsulated Nb (bottom). Nb positions are in blue, WO_6 octahedra are in cyan, oxo ligands are red.

The final composition of the anion can be written as $[P_8W_{48}O_{184}\{NbO(H_2O)\}_{0.4}\{NbO(H_2O)(C_2O_4)\}_{3.2}]^{35.6-}$, and, according to the elemental analysis, the total composition of **1** can be written as $Li_{4.2}(NH_4)_{31}H_{0.4}[(P_8W_{48}O_{184})(NbO(H_2O))_{3.6}(C_2O_4)_{3.2}]\cdot 64H_2O$. In the crystal structure of **1** the anions form two-layered packing with layers parallel to [110] planes. The anions are arranged in a *bcc* sublattice, typical for {P_8W_{48}} packing patterns (Fig. S1).

The combined X-ray and analytical data show that in **1,** roughly four $\{NbO(H_2O)\}^{3+}$ units occupy the two sorts of coordination sites, which differ in the coordination mode of Nb: the "common site" accommodates Nb with CN 6 (89% of total Nb), and the pentagonal site accommodates Nb with CN 7 (11% of total Nb). The heptacoordinated Nb has a pentagonal bipyramidal arrangement, just like in $(NH_4)[NbO(C_2O_4)_2(H_2O)_2]\cdot 3H_2O$ and in the structures of some polyoxoniobates and oxides [44,45]. It is worth noting that the {NbO_7} pentagonal building block behaves towards {P_8W_{48}} in a manner closely resembling the behavior of uranyl, UO_2^{2+}, which also occupies the same two types of coordination sites with less than full occupancy.[46] Other large cations, such as Ln^{3+}, might also occupy these positions, but there the situation

is more complicated: reaction of larger Ln^{3+} (La-Nd) with $[P_8W_{48}O_{184}]^{40-}$ leads not only to incorporation of two Ln^{3+}, but also of eight tungstate ions, thus radically modifying the cavity; in any case, no Ln^{3+} was detected in the pentagonal positions.[6]

Solution studies

As discussed above, the reaction of Nb-Ox with $[P_8W_{48}O_{184}]^{40-}$ leads to formation of a set of mixed $\{P_8W_{48}O_{184}\{NbO(H_2O)\}_n\}$·species, mostly with n = 3 and 4, where Nb does not occupy all the accessible coordination sites. We studied solution behavior of these complexes with ^{31}P and ^{13}C NMR (together with ^{13}C MAS NMR) techniques, in combination with HPLC-ICP-AES analytical technique [47]. Small angle X-ray scattering was also performed on compounds **B** to compare the experimental and simulated curves and estimate the positions of Nb.

In our previous research, a combination of NMR and HPLC-ICP-AES provided precise information about the behavior of mixed $[XW_{11}NbO_{40}]^{n-}$ anions in aqueous solutions.[39] It should be noted that the HPLC-ACP-AES techniques has not been used in solution studies of large polyoxoanions such as $\{P_8W_{48}\}$. The HPLC-ICP-AES data indicate the presence of two broad overlapping peaks in both series of Nb-functionalized K^+/Li^+ and NH_4^+/Li^+ salts (Fig. 4, S2; retention times are summarized in Table S1). According to ICP data the first peak has the W:Nb ratio close to 16 (three Nb atoms per anion), while the second has this ratio close to 12 (four Nb atoms per anion).

We may assume that in solution there are some equilibria involving: i) dynamic release and uptake of the $\{ONb(C_2O_4)\}^+$ by the $\{P_8W_{48}\}$ cavitands, and ii) exchanging positions within the cavity. These equilibria affect both the $\{P_8W_{48}Nb_3\}$ and $\{P_8W_{48}Nb_4\}$ species and cause broadening and partial overlap of the chromatographic peaks. Each peak corresponds to a group of positional isomers with the same charge and size and which, therefore, are extremely difficult to separate. To confirm this assumption, we recorded ^{31}P NMR spectra of all isolated solids (**A(a-e)** in Table 1; **B(a-d)** in Table 3) in aqueous solution. Two groups of overlapping signals from different positional isomers of the $\{ONb(C_2O_4)\}^+$ groups were found in all cases (Fig. S3). For the K^+/Li^+ salts the centers of each group are observed at -7.5 and -8.5 ppm. For the NH_4^+/Li^+ salts they are shifted to -8.5 and -9.5 ppm (Fig. S4). The presence of two groups of signals in ^{31}P NMR agrees well with the HPLC-ICP-AES results. Taking into account recorded upfield shifts of ^{31}P signals of $\{P_8W_{48}\}$ upon the inclusion of heteroatoms[1,8,46] we can assign both groups of peaks. The groups centered at -7.5 ppm (for K^+/Li^+) and -8.5 (for NH_4^+/Li^+) are from the species with 3 Nb atoms in the cavity, and the groups centered at -8.5 ppm (for K^+/Li^+) and -9.5 (for NH_4^+/Li^+) are from the species with 4 Nb in the cavity. Narrowness of the peaks in all spectra indicate slow exchange dynamics of Nb=O groups in NMR scale. For compound **A(e)** the ^{31}P NMR spectrum looks simpler indicating the presence of only one symmetric isomer as major product.

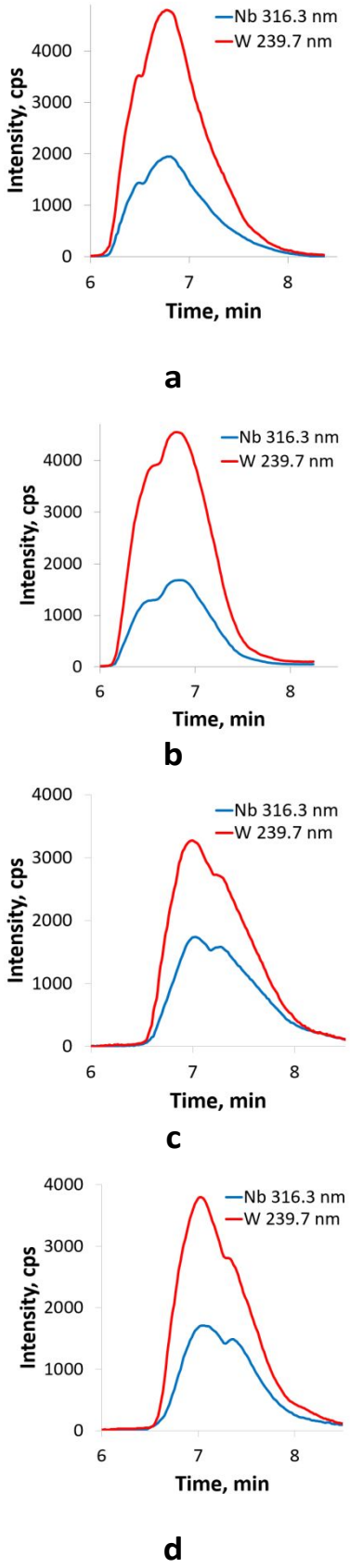

Figure 4. HPLC-ICP-AES chromatograms for NH_4^+/Li^+ salts **B(a-d)**.

Aqueous solution ^{13}C NMR spectra for all products feature a wide signal at 169.6 ppm, arising from several overlapping closely spaced signals (Fig. S5). Solids ^{13}C MAS NMR data (recorded at 15 KHz) show a multicomponent signal centered at 170 ppm, from non-equivalent oxalate anions (Fig. S6). This may reflect the different orientations of the O=Nb-OH_2 moiety (or different environment of oxalate), as discussed above, and confirms the presence of oxalate ligands coordinated to Nb residing in the "common sites".

The ESI-MS characterization of such high-nuclearity POMs is far from trivial because of their high molecular weights, high charge states, multiple isotopes, and equilibriums involving several species. Moreover, ionization involves multiple associations with various number of alkali cations and protons, as well as with water molecules.

Hence, broad and partially overlapping peak envelopes are observed in the ESI mass spectra of **B(a-d)**, which preclude accurate determination of the composition of the POMs. The Cronin group has pioneered use of ESI-MS techniques for identification of giant polyanions on the basis of the observation of polyanions with different numbers of cations and water molecules, existing as either monomers or oligomers of the related parent polyanion.[48–50] Molecular weights can be estimated by ESI-MS via deconvolution of multiply charged states of the intact polyanion, taking into account the spacing between isotopically-resolved peaks in one peak envelope corresponding to one charge state and the spacing between the series of broad peaks in the ESI-MS. In this context, the ESI mass spectra of 10^{-4} M aqueous solutions of compounds **B(a-d)** were interpreted. A typical HR-ESI-MS(-) spectrum is shown in Figure 5, which displays four broad peaks centered at m/z 1380, 1550, 1780 and 2080, encompassing 9– to 6– charge states. Modeling each peak composition is shown in Fig. 5 (bottom) and Fig. S7-S9 (examples of comparison between experimental and calculated isotopic patters are presented in Fig. S10-21). In general, accurate peak assignments were not possible because of the inherent broadness of the peaks due to the interactions with cations (H^+, Li^+, or NH_4^+) and partial removal of water molecules or oxalate anions. However, from the m/z values and the charge state determination, it is clear that the integrity of the $[P_8W_{48}O_{184}\{NbO(C_2O_4)(H_2O)\}_n]$ (n = 1-4) POM is preserved in solution in the conditions of the ESI-MS experiment. Table S2 in SI gives possible assignments of the observed peaks.

For example, modeling of the $\{P_8W_{48}Nb_5\}$ species reveals $[(P_8W_{48}O_{184})(NbO(C_2O_4)(H_2O))_5^{35-} + 26H^+]$ (m/z 1448.5); $[(P_8W_{48}O_{184})(NbO(C_2O_4)(H_2O))_5^{35-} + 20H^+ + 3Li^+ + 3NH_4^+]$ (m/z 1456.2); $[(P_8W_{48}O_{184})(NbO(C_2O_4)(H_2O))_5^{35-} + 17H^+ + 3Li^+ + 6NH_4^+]$ (m/z 1461.8), labeled as *, ** and *** respectively. However, the species with more than four $\{NbO(C_2O_4)(H_2O)\}$ groups per $\{P_8W_{48}\}$ have very low intensities in the spectra (Fig. 6). We can assume that complexes with five and more niobium containing groups are inherently unstable, in particular under high dilution required for recording ESI mass spectra, or they have rather poor ionization efficiency in ESI source.

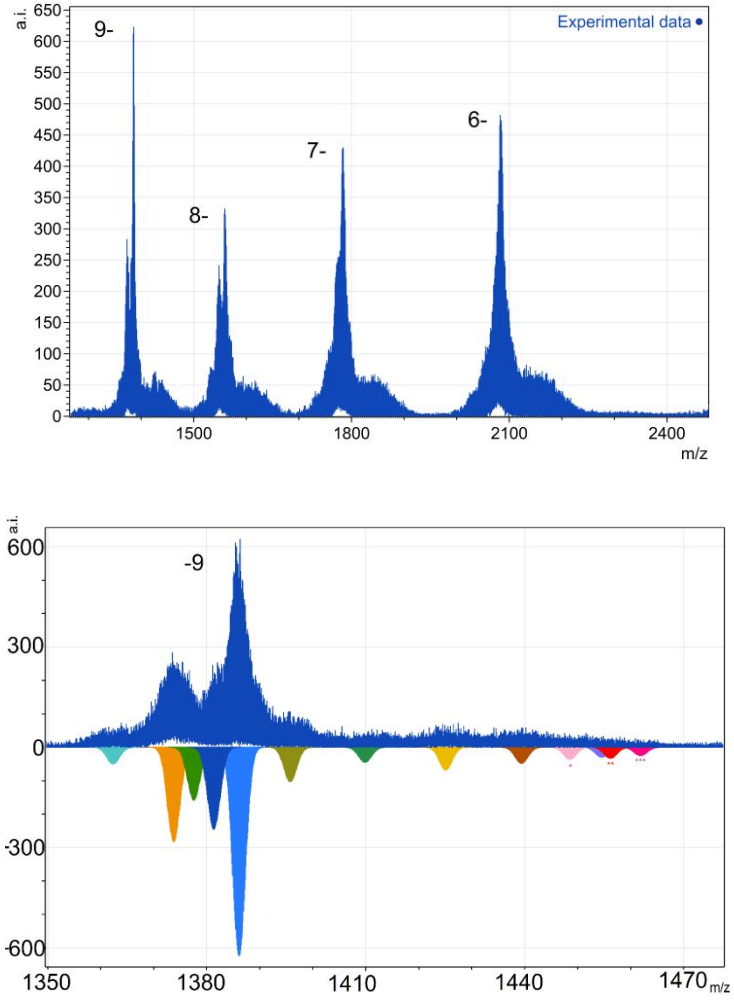

Figure 5. The typical ESI-MS(-) spectrum of **B(a-d)** (up). Modeling of observed 9- peak by overlapping of different forms (bottom), assignment is presented in Table S2.

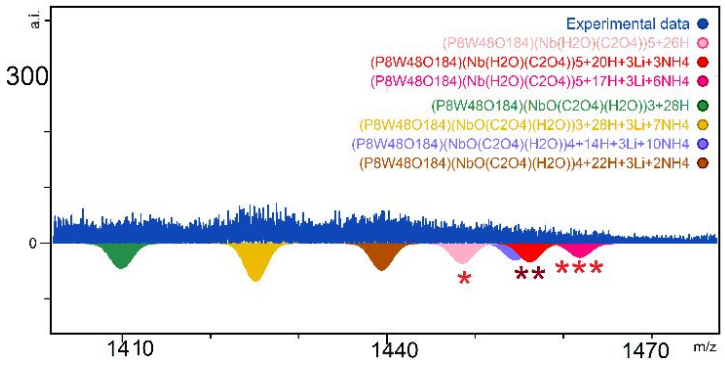

Figure 6. Modelling of observed 9- peak by overlapping of different forms with 5 $\{NbO(C_2O_4)(H_2O)\}$ groups.

Small angle X-ray scattering (SAXS) is a technique that is gaining popularity to determine the size and the shape of POMs in solution.[51] Relevant to the current study, SAXS is particularly sensitive to core-shell structures of capsule topologies,[52] and the encapsulated contents such as Nb-intercalated P_8W_{48}. In this work, we corroborated the location of the niobium atoms in compounds **B(a)**, **B(c)** and **B(d)** via SAXS (Fig. S22). We simulate the scattering curves of the 'empty' P_8W_{48} cluster, and P_8W_{48} with encapsulated Nb species, located in the two different coordination sites (called Nb_{Oh} and Nb_{pent}; respectively octahedral and pentagonal bipyramidal illustrated in figure 2 and 3). In theory, the number and the position of the encapsulated Nb slightly affects the scattering curve (Fig S23). Filling the site that is embedded in the POM (which we call Nb_{pent}, Fig. 7) has almost no effect on the simulated scattering data. On the other hand, increasing Nb concentration in the common site (Nb_{Oh}, Fig. 7) leads to suppression in the first oscillation (q=0.3-0.7 $Å^{-1}$), as well as subsequent oscillations (q=0.7-2.5 $Å^{-1}$) (Fig. S11). This effect has been noted prior, in both simulation and experiment.[52] We will focus on the first oscillation in our interpretations, since the subsequent oscillations can be affected by solvent scattering. However, notably, the oscillations of the simulated data also match well with the experimental data, which is a testament to the purity of the samples—meaning no other W-Nb POM topologies are present in solution.

On the other hand, there is a considerable misalignment at q<0.2 $Å^{-1}$ between the simulated and experimental data for all samples, while the Guinier region matches well (q=0.2-0.4 $Å^{-1}$). We attribute this to a structure factor in the experimental data, due to high concentration of the dissolved POM. The data could not be modeled exactly by pair distance distribution function (PDDF); the calculated model showed an increased intensity deviation at q<0.2 $Å^{-1}$ (Fig. S24). However, the resulting PDDF (fig. 8, discussed later) profiles accurately represent a cluster with high electron density in the shell and less electron density in the core. A simple spherical model fit could be used that required inclusion of a structure factor, which describes the distance between scattering species and the approximate number of 'nearest neighbors (respectively 24.8 and 0.47; see Fig. S25). Structure refinement of **1** (composition close to sample **B(d)**) revealed 3.2 octahedral Nb and 0.4 pentagonal Nb incorporated in the POM. However, the presence of Nb located in the pentagonal site (Nb_{pent}) does not change the scattering curve in the Guinier region. The scattering of compounds **B(a)** and **B(d)** are very similar to each other, and both the Guinier region and first oscillation match that of simulated P_8W_{48} containing four niobium atoms located on the common site (Nb_{Oh}, Fig. 7 top; expected 4.1 and 3.6 Nb respectively). This data indicates that in solution, the majority of Nb atoms are present in the common site, but it is also possible Nb atoms are in the pentagonal geometry, as shown by refinement of the X-ray data. The scattering curve of compound **B(c)** is different from the two others and shows a better match to the simulated data with eight Nb atoms in the common site, different from other characterization that support incorporation of 5 Nb.

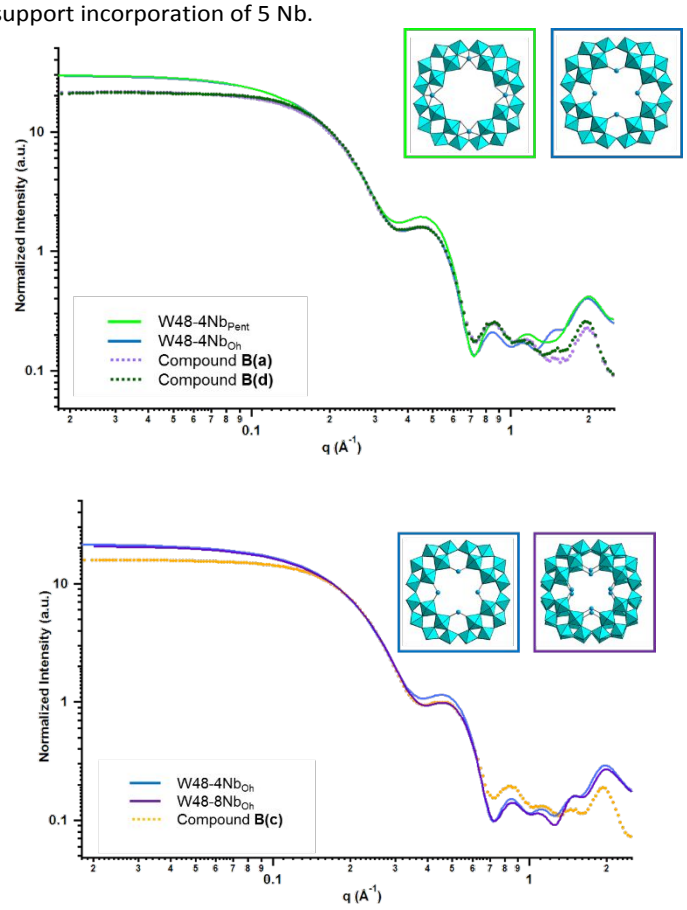

Figure 7. Experimental SAXS curves of compounds **B(a)** and **B(d)** (top) and **B(c)** (bottom), along with simulated scattering curves of P_8W_{48} incorporating 4 Nb in the pentagonal position (light green), 4 Nb in the common site (blue) or 8 Nb in the common site (purple). Simulated scattering curves are represented as solid lines while experimental scattering curves are dotted lines.

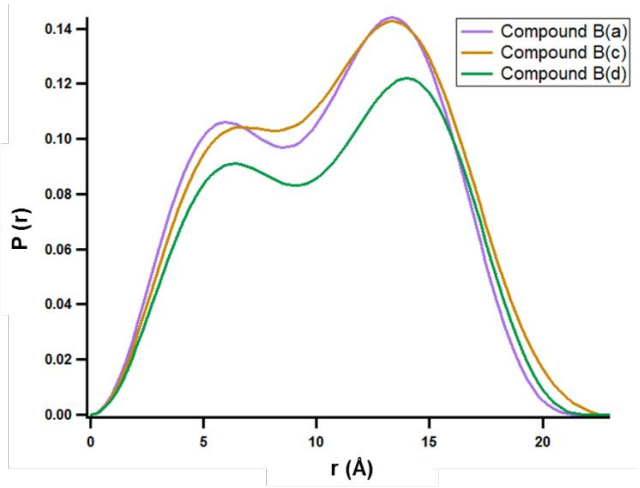

Figure 8. The PDDF of compounds **B(a)**, **B(c)** and **B(d)**.

Consistent with the NMR studies, this suggests the Nb in solution can exchange sites. The observed SAXS data suggests

the Nb moves more towards the center of the cavitand, decreasing the electron density contrast between the shell and the core (and thus suppressing the feature between q=0.3-0.7 $Å^{-1}$).

The PDDF analysis of experimental and simulated scattering curves provides a real space representation of the capsule geometry with increasing Nb-incorporation. A PDDF is a probability map of scattering vectors through the clusters, where scattering power of the elements, and probability of scattering length contribute to the intensity (Fig. 8). Both experimental (Fig. 8) and simulated (Fig. S26**)** PDDFs show an approximate Gaussian distribution with a shoulder on the left. This is the typical profile for core-shell type structures with greater electron density in the shell. Moreover, the maximum linear extent of all the PDDFs agree with the diameter of the capsule measured from the X-ray structure (~23 Å diameter; see Table S4). Notably, the PDDF for **B(c)** which contains the most Nb in the cavity has the most featureless profile. It has a less pronounced shoulder, indicating less electron density contrast between the shell and the core. In summary, SAXS is sensitive to the small differences of Nb content and position in the capsule, and is a powerful tool for monitoring dynamic capsules such as W_{48}.

Conclusions

Incorporation of Nb into the $[P_8W_{48}O_{184}]^{40-}$ anionic macrocyclic cavitand leads to formation of a series of new Nb-W POM. There are in total at least eight equivalent accessible sites for binding Nb and other transition metals ("common sites"). K^+ and Li^+ cations always present as counter cations to balance the high negative charge of $[P_8W_{48}O_{184}]^{40-}$ successfully compete with Nb(V) and prevent incorporation of more than five Nb(V) centers (K^+ competes more successfully than Li^+). Usually, three and four Nb(V) centers are encapsulated, randomly occupying available coordination sites. A minor fraction of Nb(V) also enters vacant pentagonal positions, which are typically left free when coordination of 3d cations takes place. The complexes are labile, and in solution there is a set of equilibria including species with fewer number of niobium atoms per $\{P_8W_{48}\}$. The SAXS data indicate the Nb migrates from pentagonal to the "common site" in solution, thus filling the central cavity. With $[NbO(C_2O_4)_2(H_2O)_2]^-$ as Nb source, Nb tends to be incorporated as $\{ONb(H_2O)(C_2O_4)\}^+$ moiety. This extra oxalate can be used to anchor other metal ions, and the labile Nb-bound water provides either a site for catalytic reactions, ligand exchange, or linking to other metal centers.

Experimental

General information

$K_{28}Li_5H_7[P_8W_{48}O_{184}]\cdot 92H_2O$ or $Li_{17}(NH_4)_{21}H_2[P_8W_{48}O_{184}]\cdot 85H_2O$ were synthesized according to literature methods.[53,54] Nb-Ox was purchased from Sigma Aldrich. Other reagents were of commercial quality and were used as purchased. Elemental analysis was carried out on a Eurovector EA 3000 CHN analyzer. NMR spectra were run on a Bruker Avance III 500 spectrometer at room temperature with addition of a very small amount of D_2O to the sample aqueous solutions. ^{13}C MAS NMR spectra were recorded on a Bruker Avance III 500 spectrometer at room temperature at 15KHz. FT-IR spectra were recorded on a FT-801 spectrometer (Simex, Russia). TGA experiments were done on a NETZSCH TG 209 F1 device in an Al crucible by heating a sample from 20 to 300 °C with 10 °C gradient.

$K_xLi_yH_z[(P_8W_{48}O_{184})(NbO(H_2O))_n(C_2O_4)_m]\cdot XXH_2O$ (A-set):

Calculated amount of Nb-Ox was added to a suspension of 0.400 g (0.027 mmol) $K_{28}Li_5H_7[P_8W_{48}O_{184}]\cdot 92H_2O$ in required volume of distilled water. The clear stirred solution was heated for 2 hours at 60 °C. Twelve hours after cooling to room temperature, large colorless crystals of the product were collected by vacuum filtration and air dried. All information concerning the synthesis is summarized in Table 1, analytical data are presented in Table 2. Typical IR (ν, cm^{-1}): 3355 (w), 1613 (w), 1414 (w), 1134 (m), 1080 (m), 1019 (w), 954 (sh), 910 (s), 815 (s), 633 (vs).

$Li_x(NH_4)_yH_z[(P_8W_{48}O_{184})(NbO(H_2O))_n(C_2O_4)_m]\cdot XXH_2O$ (B-set)

Calculated amount of Nb-Ox was added to a clear solution of 0.400 g (0.029 mmol) $Li_{17}(NH_4)_{21}H_2[P_8W_{48}O_{184}]\cdot 85H_2O$ in required volume of distilled water. The reaction mixture was heated for 2 hours at 60 °C under stirring. After cooling to room temperature the reaction solution was stored at 5 °C. Large colorless crystals started to appear in 12 hours. They were collected by filtration and air dried. All information pertaining to the synthesis is summarized in Table 3, analytical data is presented in Table 4. Typical IR (ν, cm^{-1}): 3401 (m). 3173 (s), 2985 (s), 1681 (m), 1405 (s), 1126 (m), 1079 (m), 1018 (s), 982 (w), 908 (s), 796 (s), 648 (vs). The product isolated from the reaction with $Li_{17}(NH_4)_{21}H_2[P_8W_{48}O_{184}]\cdot 85H_2O$ at the $\{Nb\text{-}Ox\}/\{P_8W_{48}\}$ = 30:1 ratio was marked as (**1**).

Single-crystal X-ray diffraction

Crystallographic data and refinement details for **1** are given in Table S3 (see Electronic supplementary information). The diffraction data were collected on a New Xcalibur (Agilent Technologies) diffractometer with MoK_α radiation (λ = 0.71073) by doing ϕ scans of narrow (0.5°) frames at 130 K. Absorption correction was done empirically using SCALE3 ABSPACK (CrysAlisPro, Agilent Technologies, Version 1.171.37.35 (release 13-08-2014 CrysAlis171 .NET)). Structure was solved by direct method and refined by full-matrix least-squares treatment against $|F|^2$ in anisotropic approximation with SHELX 2017/1 [55] in ShelXle program.[56] Hydrogen atoms of NH_4^+ and water molecules of crystallization were not located.

ARTICLE

Table. 1. Experimental conditions for preparation of Nb functionalized $\{P_8W_{48}\}$ anions isolated as K^+/Li^+ salts.

Name	m(mg) Nb-Ox	Nb-Ox:$\{P_8W_{48}\}$ ratio	V(mL) H_2O; **pH**	Formula	Yield(mg)
A(a)	0.082	8:1	10; 3.5	$K_{25.7}Li_5(NH_4)_5[(HP_8W_{48}O_{184})(NbO(C_2O_4)(H_2O))_{3.3}]\cdot 73H_2O$	0.123
A(b)	0.041	4:1	10; 4.3	$K_{30.8}Li_{3.5}(NH_4)_3[(P_8W_{48}O_{184})(NbO(C_2O_4)(H_2O))_{1.7}]\cdot 74.5H_2O$	0.083
A(c)	0.164	16:1	10; 2.0	$K_{21.6}Li_5(NH_4)_8H_{6.8}[(P_8W_{48}O_{184})(NbO(H_2O))_{4.4}(C_2O_4)_{1.5}]\cdot 66H_2O$	0.140
A(d)	0.082	8:1	5; 3.2	$K_{24.4}Li_5(NH_4)_{5.5}[(HP_8W_{48}O_{184})(NbO(C_2O_4)(H_2O))_{3.1}]\cdot 59H_2O$	0.154
A(e)	0.082	8:1	15; 3.7	$K_{26.7}Li_4(NH_4)_{5.5}H_{2.6}[(P_8W_{48}O_{184})(NbO(H_2O))_{3.8}(C_2O_4)_{2.5}]\cdot 55.5H_2O$	0.109

Table. 2. Analytical data for Nb functionalized $\{P_8W_{48}\}$ anions isolated as K^+/Li^+ salts.

Name	Found							Calcd.							TGA loss (%) 25-300
	C	H	N	K	Li	W	Nb	C	H	N	K	Li	W	Nb	
A(a)	0.5	0.9	0.5	6.5	0.2	58.2	2.1	0.52	1.2	0.46	6.6	0.23	58.2	2.0	10.8
A(b)	0.3	0.9	0.3	8.1	0.2	58.5	1.3	0.28	1.1	0.28	8.0	0.16	58.8	1.1	10.5
A(c)	0.3	1.0	0.7	5.6	0.2	58.9	2.6	0.24	1.2	0.75	5.7	0.23	59.1	2.7	9.1
A(d)	0.6	1.3	0.5	6.5	0.2	59.3	1.8	0.50	1.0	0.52	6.4	0.23	59.5	1.9	10
A(e)	0.6	1.2	0.5	7.1	0.2	59.4	2.5	0.51	1.0	0.52	7.0	0.19	59.3	2.4	8.8

Table. 3. Experimental conditions for preparation of Nb functionalized $\{P_8W_{48}\}$ anions isolated as NH_4^+/Li^+ salts.

Name	m(mg) Nb-Ox	Nb-Ox/$\{P_8W_{48}\}$ ratio	V(mL) H_2O; **pH**	Formula	Yield (mg)
B(a)	0.082	8:1	5; 4.0	$Li_{3.3}(NH_4)_{29}H_5[(P_8W_{48}O_{184})(NbO(C_2O_4)(H_2O))_{4.1}(C_2O_4)_{3.4}]\cdot 57H_2O$	0.132
B(b)	0.046	4:1	5; 4.8	$Li_{3.5}(NH_4)_{30}H_{1.1}[(P_8W_{48}O_{184})(NbO(H_2O))_{2.8}(C_2O_4)_{1.5}]\cdot 57.5H_2O$	0.093
B(c)	0.184	16:1	5; 2.5	$Li_3(NH_4)_{30}[(P_8W_{48}O_{184})(NbO(H_2O))_5(C_2O_4)_4]\cdot 59H_2O$	0.220
B(d)	0.082	8:1	2.5; 3.8	$Li_{4.2}(NH_4)_{31}H[(P_8W_{48}O_{184})(NbO(H_2O))_{3.6}(C_2O_4)_3]\cdot 64H_2O$	0.172

Table. 4. Analytical data for Nb functionalized $\{P_8W_{48}\}$ anions isolated as NH_4^+/Li^+ salts.

Name	Found						Calcd.						TGA loss (%) 25-300
	C	H	N	Li	W	Nb	C	H	N	Li	W	Nb	
B(a)	0.3	1.7	2.8	0.18	61.3	2.6	0.4	1.68	2.83	0.17	61.6	2.7	13.0
B(b)	0.2	1.8	2.9	0.18	62.3	1.9	0.26	1.73	2.98	0.17	62.5	1.8	13.2
B(c)	0.6	1.6	2.9	0.12	60.1	3.1	0.66	1.71	2.87	0.14	60.3	3.2	14.5
B(d)	0.5	1.8	3.0	0.18	60.8	2.4	0.5	1.8	3.0	0.20	60.9	2.3	14.4

The numbers of NH_4^+, Li^+ cations, oxalate anions and water molecules of crystallization were found from analytical data and the composition of **1** is close to **B(d)**. The crystallographic data have been deposed in the Cambridge Crystallographic Data Centre under the deposition codes CCDC 1862500 (**1**).

HPLC-ICP-AES

Separations were performed with HPLC system Milichrom A-02 (EcoNova, Russia) equipped with a two-beam spectrophotometric detector at the wavelength range of 190–360 nm in ion-pair mode of reversed phase chromatography (ProntoSIL 120-5-C18AQ, 2x75 mm). Taking into account the limitations of the stability of POMs, an acidic buffer was used as mobile phase. Preference was given to the acetate buffer (pH 4.5) and 0.04% tetrabutylammonium hydroxide (TBAH) as an ion-pair agent (eluent A) in order to secure the regular peak shape and acetonitrile (eluent B). Good quality separation in terms of efficiency, peak shape and retention time was achieved in gradient mode with gradual increase in acetonitrile concentration. The gradient mode conditions: 0–3.3 min, 0–30% B; 3.3–10.3 min, 30–55% B; 10.3–16.7 min, 55% B; flow rate – 0.18 mL min^{-1}. Detection wavelength: 250 nm. An ICP-AES spectrometer iCap 6500 Duo (Thermo Scientific, USA) with concentric nebulizer was applied as detector in hyphenated HPLC-ICP-AES mode. For quantitative estimations the Nb 316.3 nm, W 239.7 nm spectral lines were selected. All measurements were performed in three replicates. The data acquisition and processing was carried out with iTEVA (Thermo Scientific, USA) software. The ICP-AES working parameters: power supply – 1150 W, nebulizer Ar flow rate – 0.70 L min^{-1}, auxiliary – 0.50 L min^{-1}, cooling – 12 L min^{-1}. In order to eliminate plasma quenching we diluted the liquid coming out of the column into the spray chamber with deionized water. The steady state of the plasma and the optimal values of analytical signals were finally achieved at the eluent flow rate of 0.18 mL min^{-1}, and the eluent velocity of 3 mL min^{-1} (peristaltic pump speed – 75 rpm). Under these conditions, stable plasma burning was observed even when the share of acetonitrile in the gradient profile attained 55%.

HR-ESI-MS

The high-resolution electrospray ionization mass spectrometric (HR-ESI-MS) detection was performed with a direct injection of liquid samples on an ESI quadrupole time-of-filght (ESI-q-TOF) high-resolution mass spectrometer Maxis 4G (Bruker Daltonics, Germany). The spectra were recorded in the 300-3000 m/z range in negative mode.

SAXS

Scattering data were collected on an Anton Paar SAXSess instrument utilizing Cu- Ka radiation (1.54 Å) and line collimation. Ten millimolar solutions of **B(a)**, **B(c)** and **B(d)** were prepared by dissolving the compounds in weak nitric acid (to enable solubility) and sealed in a 1.5 mm diameter borosilicate capillary. The data was collected in an evacuated X-ray chamber for 30 min. Data were processed using SAXSquant software for normalization, background subtraction, desmearing, and smoothing. Analysis of the processed data was carried out using Igor Pro with the Irena macros.[57] SolX software was used for creating simulated scattering curves.[58]

Conflicts of interest

There are no conflicts to declare.

Acknowledgements

This work was supported by Russian Science Foundation (grant number 14-13-00645). NM and MN performed the SAXS analysis and interpretation with support from the U.S. Department of Energy, Office of Basic Energy Sciences, Division of Material Sciences and Engineering (Award DE SC0010802). VY acknowledges Ministry of science and higher education of RF (№ 0333-2017-0002).

Notes and references

1 N. V. Izarova, L. Klaß, P. de Oliveira, I.-M. Mbomekalle, V. Peters, F. Haarmann and P. Kögerler, *Dalton Trans.*, 2015, **44**, 19200–19206.
2 S. G. Mitchell, D. Gabb, C. Ritchie, N. Hazel, D.-L. Long and L. Cronin, *CrystEngComm*, 2009, **11**, 36–39.
3 S. S. Mal, N. H. Nsouli, M. H. Dickman and U. Kortz, *Dalton Trans.*, 2007, **0**, 2627–2630.
4 S. S. Mal and U. Kortz, *Angew. Chemie Int. Ed.*, 2005, **44**, 3777–3780.
5 L. Chen, J. Hu, S. S. Mal, U. Kortz, H. Jaensch, G. Mathys and R. M. Richards, *Chem. - A Eur. J.*, 2009, **15**, 7490–7497.
6 M. Zimmermann, N. Belai, R. J. Butcher, M. T. Pope, E. V. Chubarova, M. H. Dickman and U. Kortz, *Inorg. Chem.*, 2007, **46**, 1737–1740.
7 X. Fang, P. Kögerler, Y. Furukawa, M. Speldrich and M. Luban, *Angew. Chemie Int. Ed.*, 2011, **50**, 5212–5216.
8 V. S. Korenev, S. Floquet, J. Marrot, M. Haouas, I.-M. Mbomekallé, F. Taulelle, M. N. Sokolov, V. P. Fedin and E. Cadot, *Inorg. Chem.*, 2012, **51**, 2349–2358.
9 N. Watfa, S. Floquet, E. Terazzi, M. Haouas, W. Salomon, V. S. Korenev, F. Taulelle, L. Guénée, A. Hijazi, D. Naoufal, C. Piguet and E. Cadot, *Soft Matter*, 2015, **11**, 1087–1099.
10 S. G. Mitchell, C. Streb, H. N. Miras, T. Boyd, D.-L. Long and L. Cronin, *Nat. Chem.*, 2010, **2**, 308–312.
11 L. Li, J. Deng, R. Yu, J. Chen, Z. Wang and X. Xing, *J. Mater. Chem. A*, 2013, **1**, 11894.
12 Y. Zhang, L. Pei, Z. Zheng, Y. Yuan, T. Xie, J. Yang, S. Chen, J. Wang, E. R. Waclawik and H. Zhu, *J. Mater. Chem. A*, 2015, **3**, 18045–18052.
13 A. A. Shmakova, E. M. Glebov, V. V. Korolev, D. V. Stass, E. Benassi, P. A. Abramov and M. N. Sokolov, *Dalton Trans.*,

2018, **47**, 2247–2255.
14 J. Niu, F. Li, J. Zhao, P. Ma, D. Zhang, B. Bassil, U. Kortz and J. Wang, *Chem. - A Eur. J.*, 2014, **20**, 9852–9857.
15 D. Zhang, Z. Liang, S. Xie, P. Ma, C. Zhang, J. Wang and J. Niu, *Inorg. Chem.*, 2014, **53**, 9917–9922.
16 M. K. Kinnan, W. R. Creasy, L. B. Fullmer, H. L. Schreuder-Gibson and M. Nyman, *Eur. J. Inorg. Chem.*, 2014, 2361–2367.
17 A. L. Kaledin, D. M. Driscoll, D. Troya, D. L. Collins-Wildman, C. L. Hill, J. R. Morris and D. G. Musaev, *Chem. Sci.*, 2018, **9**, 2147–2158.
18 F. Bannani, H. Driss, R. Thouvenot and M. Debbabi, *J. Chem. Crystallogr.*, 2006, **37**, 37–48.
19 T. M. Anderson, M. A. Rodriguez, T. A. Stewart, J. N. Bixler, W. Xu, J. B. Parise and M. Nyman, *Eur. J. Inorg. Chem.*, 2008, 3286–3294.
20 K. Bouadjadja-Rohan, C. Lancelot, M. Fournier, A. Bonduelle-Skrzypczak, A. Hugon, O. Mentré and C. Lamonier, *Eur. J. Inorg. Chem.*, 2015, **2015**, 2067–2075.
21 P. I. Molina, D. J. Sures, P. Miró, L. N. Zakharov and M. Nyman, *Dalton Trans.*, 2015, **44**, 15813–15822.
22 A. Stein, M. Fendorf, T. P. Jarvie, K. T. Mueller, A. J. Benesi and T. E. Mallouk, *Chem. Mater.*, 1995, **7**, 304–313.
23 E. V. Radkov and R. H. Beer, *Inorg. Chim. Acta*, 2000, **297**, 191–198.
24 Y. Ren, Y. Hu, Y. Shan, Z. Kong, M. Gu, B. Yue and H. He, *Inorg. Chem. Commun.*, 2014, **40**, 108–111.
25 A. Trovarelli and R. G. Finke, *Inorg. Chem.*, 1993, **32**, 6034–6039.
26 C. C. Li, S. X. Liu, S. J. Li, Y. Yang, H. Y. Jin and F. J. Ma, *Eur. J. Inorg. Chem.*, 2012, 3229–3234.
27 D. A. Judd, J. H. Nettles, N. Nevins, J. P. Snyder, D. C. Liotta, J. Tang, J. Ermolieff, R. F. Schinazi and C. L. Hill, *J. Am. Chem. Soc.*, 2001, **123**, 886–897.
28 M. K. Harrup and C. L. Hill, *J. Mol. Catal. A Chem.*, 1996, **106**, 57–66.
29 D. Zhang, C. Zhang, P. Ma, B. S. Bassil, R. Al-Oweini, U. Kortz, J. Wang and J. Niu, *Inorg. Chem. Front.*, 2015, **2**, 254–262.
30 Patent US 07/257, 1991, 891.
31 R. G. Finke and M. W. Droege, *J. Am. Chem. Soc.*, 1984, **106**, 7274–7277.
32 X. López, C. Bo and J. M. Poblet, *J. Am. Chem. Soc.*, 2002, **124**, 12574–12582.
33 K. Nomiya, C. Nozaki, A. Kano, T. Taguchi and K. Ohsawa, *J. Organomet. Chem.*, 1997, **533**, 153–159.
34 G.-S. S. Kim, D. A. Judd, C. L. Hill and R. F. Schinazi, *J. Med. Chem.*, 1994, **37**, 816–820.
35 N. Satake, T. Hirano, K. Kamata, K. Suzuki, K. Yamaguchi and N. Mizuno, *Chem. Lett.*, 2015, **44**, 899–901.
36 D. R. Park, S. Park, Y. Bang and I. K. Song, *Appl. Catal. A Gen.*, 2010, **373**, 201–207.
37 E. Cadot, V. Béreau and F. Sécheresse, *Inorg. Chim. Acta*, 1995, **239**, 39–42.
38 P. A. Abramov, A. A. Shmakova, M. Haouas, G. Fink, E. Cadot and M. N. Sokolov, *New J. Chem.*, 2017, **41**, 256–262.
39 A. A. Shmakova, M. M. Akhmetova, V. V. Volchek, T. E. Romanova, I. Korolkov, D. G. Sheven, S. A. Adonin, P. A. Abramov and M. N. Sokolov, *New J. Chem.*, 2018, **42**, 7940–7948.
40 A. A. Shmakova, T. E. Romanova, N. B. Kompankov, P. A. Abramov and M. N. Sokolov, *Eur. J. Inorg. Chem.*, , DOI:10.1002/ejic.201900209.
41 G.-S. Kim, H. Zeng, W. A. Neiwert, J. J. Cowan, D. VanDerveer, C. L. Hill and I. A. Weinstock, *Inorg. Chem.*, 2003, **42**, 5537–5544.
42 A. Müller, P. Kögerler and A. W. M. W. M. Dress, *Coord. Chem. Rev.*, 2001, **222**, 193–218.
43 A. Müller and C. Serain, *Acc. Chem. Res.*, 2000, **33**, 2–10.
44 R. Tsunashima, D. L. Long, H. N. Miras, D. Gabb, C. P. Pradeep and L. Cronin, *Angew. Chemie - Int. Ed.*, 2010, **49**, 113–116.
45 P. A. Abramov, A. T. Davletgildeeva, N. K. Moroz, N. B. Kompankov, B. Santiago-Schübel and M. N. Sokolov, *Inorg. Chem.*, 2016, **55**, 12807–12814.
46 M. N. Sokolov and V. S. Korenev, *Russ. J. Inorg. Chem.*
47 O. V. Shuvaeva, A. A. Zhdanov, T. E. Romanova, P. A. Abramov and M. N. Sokolov, *Dalton Trans.*, 2017, **46**, 3541–3546.
48 J. Gao, J. Yan, S. Beeg, D. L. Long and L. Cronin, *J. Am. Chem. Soc.*, 2013, **135**, 1796–1805.
49 J. Yan, J. Gao, D.-L. Long, H. N. Miras and L. Cronin, *J. Am. Chem. Soc.*, 2010, **132**, 11410–11411.
50 J. Gao, J. Yan, S. Beeg, D.-L. Long and L. Cronin, *Angew. Chemie Int. Ed.*, 2012, **51**, 3373–3376.
51 M. Nyman, *Coord. Chem. Rev.*, 2017, **352**, 461–472.
52 O. Renier, C. Falaise, H. Neal, K. Kozma and M. Nyman, *Angew. Chemie*, 2016, **128**, 13678–13682.
53 R. Contant and A. Teze, *Inorg. Chem.*, 1985, **24**, 4610–4614.
54 T. Boyd, S. G. Mitchell, D. Gabb, D. L. Long and L. Cronin, *Chem. - A Eur. J.*, 2011, **17**, 12010–12014.
55 G. M. Sheldrick, *Acta Cryst. Sect. A Found. Adv.*, 2015, **71**, 3–8.
56 C. B. Hübschle, G. M. Sheldrick and B. Dittrich, *J. Appl. Crystallogr.*, 2011, **44**, 1281–1284.
57 J. Ilavsky and P. R. Jemian, *J. Appl. Crystallogr.*, 2009, **42**, 347–353.
58 R. Zhang, P. Thiyagarajan and D. M. Tiede, *J. Appl. Crystallogr.*, 2000, **33**, 565–568.

SYNOPSIS. Incorporation of Nb into the $[P_8W_{48}O_{184}]^{40-}$ anionic macrocyclic cavitand leads to formation of new Nb-W POM. Inclusion of up to five $\{NbO(H_2O)\}^{3+}$ groups was observed. Solution speciation of the Nb-encapsulated macrocycles was studied by

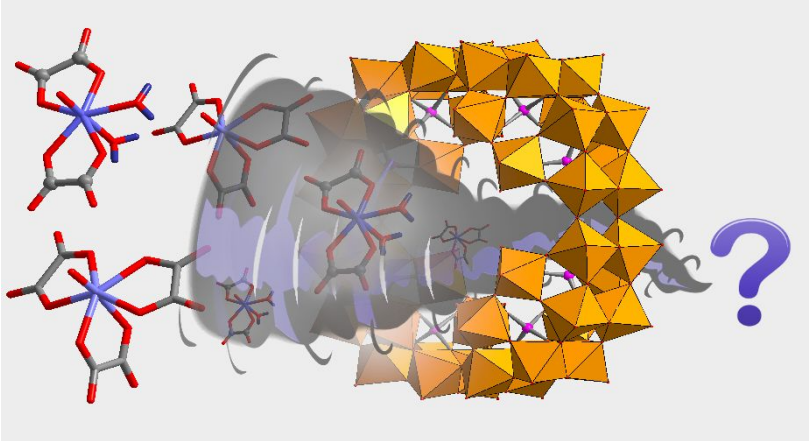

HPLC-ICP-AES and SAXS.